Desalination and Water Treatment
www.deswater.com
doi: 10.5004/dwt.2021.27941

244 (2021) 325–342
December

Adsorption of Naphthol green B on CPC modified zeolite from solution and secondary adsorption toward Methylene blue

Zhiqiang Wang[a], Jinghua Zhang[b,*], Haojiang Wang[a], Runping Han[a,*]

[a]*College of Chemistry, Green Catalysis Center, Zhengzhou University, No. 100 of Kexue Road, Zhengzhou 450001, China, emails: rphan67@zzu.edu.cn (R. Han), 445876451@qq.com (Z. Wang), wanghaojiang97@163.com (H. Wang)*
[b]*Department of Chemistry and Chemical Engineering, Huanghuai University, No. 599 of Wenhua Road, Zhumadian 463000, China, email: hollyli@126.com*

Received 12 June 2021; Accepted 25 October 2021

ABSTRACT

Removal of dyes from solution is important and low-cost materials as adsorbents are often considered in this field. In this work, the natural zeolite (NZ) was modified by hexadecylpyridinium chloride (CPC) to improve the adsorption capacity toward Naphthol green B (NGB, metal complex dye) and the exhausted adsorbent was further explored to remove Methylene blue (MB) as secondary adsorption. The characteristics of zeolite were carried out by Fourier-transform infrared spectroscopy, X-ray diffraction and Brunauer–Emmett–Teller. The adsorption behaviors of NGB on CPC modified natural zeolite (CZ) were investigated in batch mode. The adsorption quantity toward NGB from experiments was to 20.0 mg g^{-1} at 313 K (pH = 7.0, dose 1.0 g L^{-1}, dye concentration 160 mg L^{-1}). The adsorption isotherm curves of NGB onto CZ followed Freundlich, Henry, Koble–Corrigan models while kinetic curves were described using pseudo-second-order kinetic model and Elovich equation, suggesting that chemisorption and ion exchange may exist in NGB adsorption. Then, the NGB-loaded CZ (CZ-NGB) was observed to be enough stable within a wide pH range so that the materials were suitable to be applied in secondary adsorption as a new adsorbent for MB adsorption. The Redlich–Peterson and Koble–Corrigan models were confirmed to be better to depict the MB adsorption behaviors. This indicated that MB adsorption was not homogeneous. The kinetic curves of MB adsorption were in agreement with intraparticle diffusion model and double constant. The mechanism of dyes adsorption includes electrostatic attraction, ion exchange, hydrophobic interaction and Van der Waals' force. CZ is promising to remove NGB from solution and NGB-loaded CZ is also effective to bind MB from solution.

Keywords: Modified zeolite; Adsorption; Naphthol green B; Methylene blue

1. Introduction

Nowadays, the pollution from various dyes has brought about huge challenge for environment. More than 10,000 chemically different dyes have been manufactured [1,2]. Metal-complex dyes, as an important class of dyes, have been widely used in traditional technology including textile dyeing, coloring polyamide fibers, cosmetic, paper printing, drug, food, or frontier applications as key functional materials, such as with high density memory storages (CD-R and DVD-R), nonlinear optical elements [3,4]. The conventional wastewater treatments, such as flotation, coagulation, were weakly effective for dyes removal due to the extremely water-solubility and non-biodegradable of metal complex dyes [5].

Several processes have been reported for removal of metal complex dyes in water: biosorption, fungal

* Corresponding author.

decolorization, catalytic oxidation and adsorption [1,5–7]. Among these methods, adsorption has been accepted as an effective and simple technique for removal of refractory pollutants form wastewater [8,9]. Activated carbon is effective to remove various kinds of pollutants from solution, but it is too expensive and regeneration of spent activated carbon is difficult [8]. So many studies have been undertaken to investigate the use of low-cost adsorbents [8].

Zeolite is a natural, abundant and environmental friendly material. There is higher surface area and high cation exchange capacity and it has been widely used to adsorb cationic dye, phenols, ammonium and heavy metal ion, etc [9–12]. However, substitution of Si^{4+} by Al^{3+} defines the negative charge of zeolite framework, which makes zeolite prefer to combine cationic contaminants. Hence, some modified methods have been explored to remove anionic contaminant in order to expand the application of zeolite as adsorbent. Cationic surfactants can be used as modified agents to enhance the adsorption capacity of zeolite and other low-cost materials for anionic pollutants [13–16]. The cationic head groups of cationic surfactants can alter the surface negative charge of zeolite to positive charge and forming a hydrophobic layer. The anionic contaminant may combine with adsorbent through electrostatic attraction or hydrophobic. Hexadecylpyridinium chloride (CPC), as a kind of common cationic surfactant, has been reported to modify various materials to remove pollutants [17–22]. But few investigations have been reported using CPC modified zeolite (CZ) for removal of metal complex dyes.

In present work, the adsorption behavior on CPC modified zeolite toward Naphthol green B (NGB, metal complex dye) was investigated. NGB (acidic complex dye, molecular weight 878.46 g mol^{-1}, maximum absorption wavelength 714 nm) is a non-azo metal complex dye involving $-SO_3^-$ and naphthalene nucleus, indicating that this dye is good solubility and high stability. The removal of NGB with CPC modified zeolite (CZ) was performed in batch study. The effect of various important parameters on adsorption quantity, such as pH, ions strength, temperature, contact time, and initial dye concentration was investigated.

After adsorption of NGB, the usually recycling method for dye-loaded adsorbents is regenerated by water, acid, alkali in order to eliminate the contaminant on zeolite surface. But these methods may cause to second pollution. For adsorption process, the surface functional groups are crucial to affect the property of adsorbent. After reaching adsorptive saturation, the surface structures of adsorbents have been changed due to be covered by a layer of contaminations (they are stable enough in a certain condition). Hence, it can be supposed that the spent or exhausted materials as adsorbent can be further applied to remove other pollutants. That seems to be more significant for making full use of materials. Recently, the new method about reuse of the disused adsorbents had been reported as second adsorption [23,24]. But the mechanism of secondary adsorption was seldom discussed. This study aimed to explore the interaction among adsorbent, anionic dye and cationic dye so that the first and second adsorption process could be explained and the mechanism was discussed. In this work, the NGB loaded adsorbents were tried to eliminate a cationic dye, Methylene blue (MB, cationic dyes, molecular weight 319.85 g mol^{-1}, maximum absorption wavelength 665 nm). Similarly, the various factors including pH, ion strength, temperatures were investigated. Finally, the adsorption mechanisms of two dyes on adsorbents were discussed.

2. Materials and methods

2.1. Preparation of CPC modified zeolite

Zeolite was purchased from Xinyang City, Henan Province, China, whose chemical formula is $(K_2,Na_2,Ca)_3Al_6Si_{30}O_{72}\cdot 21H_2O$. Hexadecylpyridinium chloride (CPC, molecular weight 358.00 g mol^{-1}, CMC 9.0×10^{-4} mol L^{-1}) from Zhengzhou Chemical Company is chemical pure and was not treated. The modified zeolite was prepared as following [17]: the natural zeolite was milled and sieved by 40–60 mesh. Then these solids were absolutely washed and were immersed into deionized water for 24 h in constant oscillator in order to eliminate some soluble salt. After dried at 100°C, 10 g natural zeolite (NZ) was treated in 100 mL of 3% CPC at 30°C for 8 h in constant oscillator. The residual CPC concentration in the supernatant was determined using a UV/vis spectrophotometer (Shanghai Shunyu Hengping, China) at λ_{max} = 259 nm. The treated zeolite were washed by distilled water for several times until pH reached to neutral and dried in the oven at 100°C until constant weight. The final products which were named as CZ were stored in desiccators for further applications.

2.2. Characterization of CZ

Fourier-transform infrared (FTIR) analysis was used to study the surface functional groups, using FTIR spectroscope (PE-1710), where the wavelength were scanned from 4,000 to 400 cm^{-1} with a resolution of 4 cm^{-1}. The samples were dispersed in KBr and compressed into discs. X-ray diffraction (XRD) patterns were recorded using X-ray powder diffraction analyzer (BRUKER S4PIONEER, Germany).

The surface areas of NZ and CZ were determined by the N_2-BET (Brunauer–Emmett–Teller) method. The measurements were performed at 77.3 K with a volumetric adsorption analyzer (Quantan chrome NOVA1000e, USA) in relative pressures of 0.05 to 0.3. All samples were degassed for 1.5 h at 573 K prior to the vacuum volumetric.

The pH at point zero charge (pH_{pzc}) of material, namely the pH value required to give zero net surface charge of material, was evaluated by the solid addition method. For estimating the pH_{pzc} of adsorbent, a group of 0.01 g natural zeolite or CZ was treated for 12 h in an oscillator with 0.01 mol L^{-1} NaCl solution, which was as a background electrolyte. The initial pH of NaCl solution varied from 2.0 to 11.0 and was accurately measured with pH meter (Model PHS-2F), which was regularly calibrated with standard buffer solutions of pH 4.00, 6.85 and 9.18 at 303 K. In addition, the change in solid to solution ratio would lead to the change in pH_{pzc} since the charge on adsorbent surface resulted from not only the adsorption of H^+ (or OH^-) ions, but also dissolution and hydrolytic reactions taking place at the solid: solution interface [17]. Hence, the solid to solution ratio during pH_{pzc} measurement would maintain constant (1:1000). As a result, the suspensions were filtered

and final pH values were determined again. The difference between the initial pH ($pH_{initial}$) and final pH (pH_{final}) values ($\Delta pH = pH_{initial} - pH_{final}$) were plotted against $pH_{initial}$, and the point of $\Delta pH = 0$ gave the pH_{pzc}.

2.3. Preparation of NGB and MB solution

NGB and MB were selected in this study. Accurately weighted quantities of dye were dissolved in deionized water to prepare 1,000 mg L^{-1} stock solution. The further working solution of desired concentrations were obtained by diluting the stock solution. Hydrochloric acid (0.1 mol L^{-1}) and sodium hydrate (0.1 mol L^{-1}) were used to adjust solution pH if required. Other reagents used in this work are all A.R. grade reagents. Distilled water is used in all experiments.

2.4. Batch adsorption experiments for NGB onto CZ

CZ (0.05 g) was dispersed in 10 ml 80 mg L^{-1} NGB at different initial pH of 2.0–11.0. Then the suspensions were shaken by thermostatic gas-bath shaker for 12 h at 30°C and constant rotate speed. After equilibration, the mixtures were filtered and the filtrate was analyzed for residual dye concentration.

The effect of ionic strength on adsorption quantity toward NGB was investigated by various concentration of NaCl and $CaCl_2$ in NGB solution (80 mg L^{-1}). The solution pH of NGB was within 7.0–8.0 and it was not adjusted during study.

The equilibrium experiments were tested with 10 ml different initial concentration solution mixing 0.01 g adsorbent in a group of 50 ml Erlenmeyer flasks at optimum pH. The stock solution was diluted into 30–200 mg L^{-1} working solution. The flasks were shaken by thermostatic gas-bath shaker for 12 h at 20°C. The similar experiments were performed for 30°C and 40°C.

For studying the solute uptake rate on adsorbent, kinetic experiments were conducted in conical flasks containing constant volume of 30, 60, 90 mg L^{-1} NGB solution and 1.0 g L^{-1} CZ. These samples were shaken in thermostatic gas-bath shaker at constant rotate speed and were taken out at different time intervals, and then determined residual dye concentrations after solid-liquid separation. In addition, in order to make the experiments results more accurate, the above mentioned would be taken at three temperatures (293 K, 303 K, 313 K) to obtain more parameters.

The final concentrations of dye in the clear solution were determined using a UV/Vis-3000 spectrophotometer (China) with detecting maximum absorbance wavelength at 714 nm.

NGB adsorption capacity was measured from the difference between initial and final solution concentrations by using a standard calibration curve based on blanks. The adsorption experiments were performed in double and the results were expressed as average and errors less than 5%.

The adsorption capacity, q_e (mg g^{-1}), was calculated as follows:

$$q_e = \frac{(C_0 - C_e)V}{m} \quad (1)$$

where C_0 and C_e are the initial and final concentrations (mg L^{-1}), respectively, m is the adsorbent dosage (g) and V is the volume of solution (L).

2.5. Secondary adsorption experiments of MB onto CZ-NGB

After saturated adsorption of NGB, the CZ-NGB was washed by distilled water several times and dried in an oven at 60°C. The stability of CZ-NGB was explored by being immerged into a series of different pH distilled water under continuous shaking at 303 K for 12 h. The range of the initial pH values was 4.0–11.0, adjusted by 0.1 mol L^{-1} HCl or 0.1 mol L^{-1} NaOH solutions, respectively.

CZ-NGB was applied as a new sorbent in secondary adsorption experiments for removal of MB. The new adsorbent was immerged in 30 mg L^{-1} MB solution with 1.0 g L^{-1} adsorbent dosage under continuous shaking at 303 K for 12 h. The initial pH vary from 4.0 to 11.0 as NGB is not stable at pH < 4. The finial concentration of MB was measured at a maximum absorbance wavelength (665 nm).

The investigation about effects of salt concentration on removal efficiency of MB is similar to aforementioned section 2.4. Simultaneously, the effects of initial concentration and contact time, equilibrium and kinetic, also were analyzed using the similar methods of NGB adsorption.

3. Results and discussion

3.1. Characterization of NZ and CZ

3.1.1. FTIR of NZ and CZ

FTIR can be able to reflect directly the structure change of materials, namely, test the characteristic functional groups. The FTIR spectra of NZ and CZ are shown in Fig. 1.

As seen from Fig. 1, the broad and strong band in the spectrum of 3,626 cm^{-1} was attributed to H–O–H stretching vibration from water molecules weakly hydrogen bonded to the Si–O surface. The adsorption peak at 3,457 cm^{-1} was due to the –OH stretching vibration of adsorbed water. The peak associated with –OH deformation of water was verified at around 1,635 cm^{-1}. The peak observed at 1,050 cm^{-1} was due to the Si–O–Si stretching vibration.

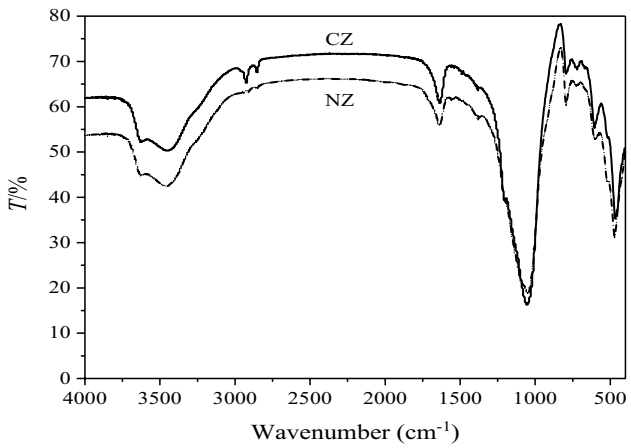

Fig. 1. FTIR spectra of natural zeolite and CZ.

The band at 794 cm^{-1} was assigned to amorphous SiO_2 stretching vibration. In addition, Si–O–Al and Si–O–Si bending vibrations were observed at 517 and 470 cm^{-1}.

For CZ, two new bands at 2,852 and 2,923 cm^{-1} (the symmetric and asymmetric stretching vibrations of $-CH_2$ and $-CH_3$) were existed in FTIR spectrum and this confirmed that the combination of natural zeolite with CPC has occurred [17]. The peak at 1,050 cm^{-1} (Si–O–Si stretching vibration) did not obviously change with CPC modification, inferring that the zeolite crystal structure remained the same as natural zeolite. Other frequency of bands only shifted slightly, which also suggested that the zeolite structure hardly altered after combination of CPC, and surfactant is existed only on the zeolite surface. Amount of CPC loaded on surface is 39.3 mg g^{-1} through measurement of CPC solution concentration before and after modification.

3.1.2. XRD of NZ and CZ

The XRD pattern (shown in Fig. 2) presented sharp reflections at low 2θ values, indicating high crystallinity [15]. The zeolite material was identified as clinoptilolite and its characteristic peaks were recognized at 2θ of 22°, 23°, 28°. Additionally, there were peaks of montmorillonite and quartz in zeolite from pattern of XRD [25].

The relative intensity of CZ peaks at 2θ of 23° decreased compared with NZ, showing that ion exchange reacting might take place in the natural zeolite when they were treated by CPC solution to some extent [26]. In addition, the mainly peaks did not obviously remove after modification, which suggesting the skeleton of zeolite change slightly and the CPC mainly load on surface of zeolite.

3.1.3. Surface area and pH of point of zero charge

Analysis of surface area was carried out by applying the BET-equation. Generally, the application of BET equation was limited in the range of low pressure (P/P_0 = 0.01–0.20). According to the experimental result (figure not shown), the N_2 adsorption volume of zeolite and CZ increased significantly when the P/P_0 increased from 0.05 to 0.30. The change tendencies of zeolite and CZ were similar, indicating that they had similar pore size distribution. The calculated BET surface area of zeolite and CZ were 25.30 and 8.50 m^2 g^{-1}, respectively. Obviously, the surface area of adsorbent decreased after CPC modified, which was due to the attachment of surfactant causing the blocking of micropore. Nevertheless, the adsorption capacity of CPC modified zeolite was still better than natural zeolite on the hydrophobicity of surfactant.

In order to evaluate the charge character of adsorbents, the pH_{pzc} of natural zeolite and CZ was measured. The pH_{pzc} value reflects surface acidity: when the adsorbent particles were immersed into a solution environment of $pH > pH_{pzc}$, their surface charge is negative; $pH < pH_{pzc}$, their surface charge is positive; $pH = pH_{pzc}$, their totally surface charge is zero.

The pH_{pzc} = 6.3 of CZ was slightly increasing compared to the pH_{pzc} = 6.1 of natural zeolite (figure not shown). It showed that the conformation of positively charged surface

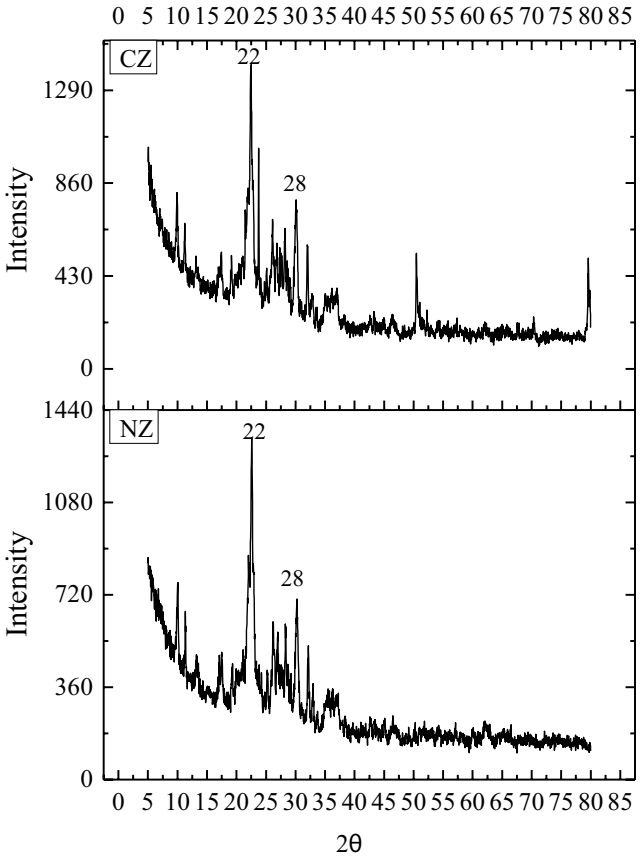

Fig. 2. XRD analysis of natural zeolite and CZ.

compounds made the surface charge of adsorbent more positive. In fact, this result was attributed to CPC as a cationic surfactant. It was also certified that CPC had been successfully loaded on the surface of natural zeolite.

3.2. NGB adsorption onto CZ

3.2.1. Effects of initial pH and salt concentration on the adsorption of NGB

The pH of the dye–CZ suspension directly affects the nature of the surface charge of adsorbent, the degree of ionization and the uptake of CZ.

The pH dependence of adsorption quantity is shown in Fig. 3a. It was found that the adsorption quantity nearly kept constant within the margin of error in first region of pH = 2.0–8.0. However, after pH 8.0, the adsorption capacity rapidly declined with the increasing basic solution. In fact, if electrostatic interaction was the only mechanism for adsorption process, the adsorption capacity should reach a maximum with the range pH 6.0–8.0 [26]. Nevertheless, in terms of the experiments, the constant adsorption quantity of CZ for NGB in pH range 2.0–8.0 inferred that the electrostatic mechanism was not the only mechanism for anionic dye adsorption in this system. As pH of origin dye solution was within 7.0–8.0, the solution pH in next work was not adjusted.

Based on the pH_{pzc} of adsorbent, the surface of CPC modified zeolite would present negative properties at pH over 6.3

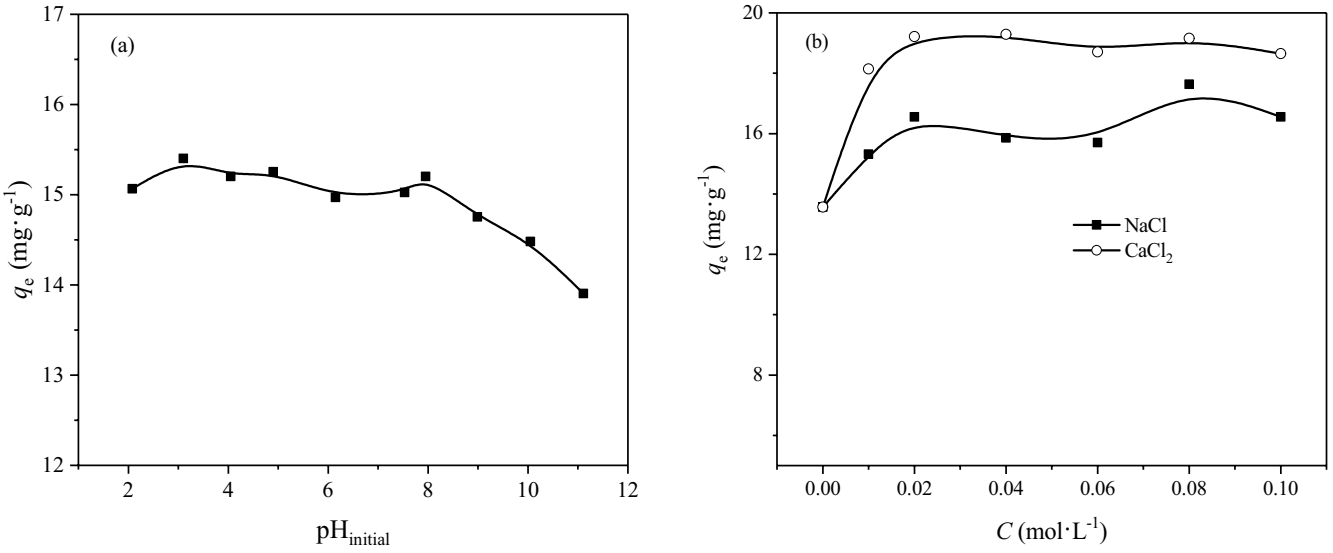

Fig. 3. (a) Effect of pH on adsorption capacity of NGB on CZ and (b) effect of salt concentration on adsorption capacity of NGB on CZ (C_0 = 80 mg L^{-1}, CZ dosage 1 g L^{-1}, t = 720 min, T = 303 K, pH 7.0 for effect of salt).

in solution. Therefore, the basic condition did not favor the adsorption due to electrostatic repulsion between the negatively charged CZ and the anionic dye molecules. Moreover, the abundance of OH^- might compete strongly with anionic NGB on active sites, which was also responsible for the lower adsorption at higher pH.

Particularly, existence of certain adsorption quantity in pH 11.0 indicated existence of other mechanism, such as intermolecular interaction or chemical sorption, beside the electrostatic interaction. The intermolecular interaction usually contains Vander Waals force and hydrogen bond.

On the other hand, the surface of zeolite loaded CPC formed a CPC layer with the positively charged head groups toward the solution. Thus, the dye molecules combined with CPC on the surface of zeolite through electrostatic interaction as the aforementioned, and they were also able to enter into CPC layer by hydrophobic interaction due to the hydrophobic nature of dye. Sun et al. reported the fly ash adsorbed Acid Black 1 from aqueous solution, which show similar trend of pH effect [27].

To investigate the effect of salt concentration on the removal of NGB by CZ, experiments were performed using NaCl and $CaCl_2$ solutions from 0.0 to 1.0 mol L^{-1} and the results are shown in Fig. 3b.

As seen from Fig. 3b, an increase in salt concentration of the medium was in favor of adsorption process and the effect of $CaCl_2$ was more than NaCl. At solution pH 7.0, dyes and the surface of CPC modified zeolite were all negative charge due to pH_{pzc} = 6.3 for CZ. Theoretically, when the electrostatic interaction is repulsive, an increase in ionic strength will enhance adsorption capacity. Usually, the particles suspended in aqueous solution do not agglomerate. This is due to the interaction of diffuse double layer. The additional electrolyte would decrease the zeta potential between boundary of particle and bulk solution so that reduce the thickness of double electrode layer. It would contribute to the increase of interaction between adsorbent and adsorbate, even aggregation.

In addition, some intermolecular forces (Van der Waals forces, ion-dipole forces, dipole-dipole forces, π–π dispersive interactions) between aromatic rings which occur between dye molecules could be able to explain this aggregation. It has been reported that these forces would increase if the addition of salt existed into the dye solution [28,29]. These reasons leaded to the increasing hydrophobic effect and dye molecules entered easily into CPC layer on zeolite.

3.2.2. Adsorption equilibrium isotherms and application of isotherm models

Adsorption isotherms are used to quantify the interaction between the adsorbate and adsorbent, which is aimed at optimizing the treatment process and giving a reference for further adsorption design in particular. The adsorption quantity at various equilibrium NGB concentrations is shown in Fig. 4.

It was noticed from Fig. 4 that adsorption quantity increased with the increase of equilibrium concentration. Moreover, the values of q_e became larger and there is in favor of NGN adsorption with the increase of temperature. This may indicate that adsorption process was endothermic.

Several two or three parameter isotherm models and kinetic models are summarized in Table 1 [30,31]. The certain parameters express the surface properties and affinity of the adsorbent. These specific parameters of adsorption systems are usually deduced from nonlinear regression using least square method with Origin 8.0 software. The coefficients of correlation (R^2) and the residual sum of squares (SSE) are selected to evaluate the models' availability.

Usually, the most popular model used to depict adsorption process is Langmuir model, which represents homogeneous and monolayer adsorption. The parameter K_L of Langmuir model showed the affinity for the binding of adsorbate. A high K_L value indicates a high affinity.

Freundlich model is based on the assumption of an exponentially declining adsorption site energy distribution.

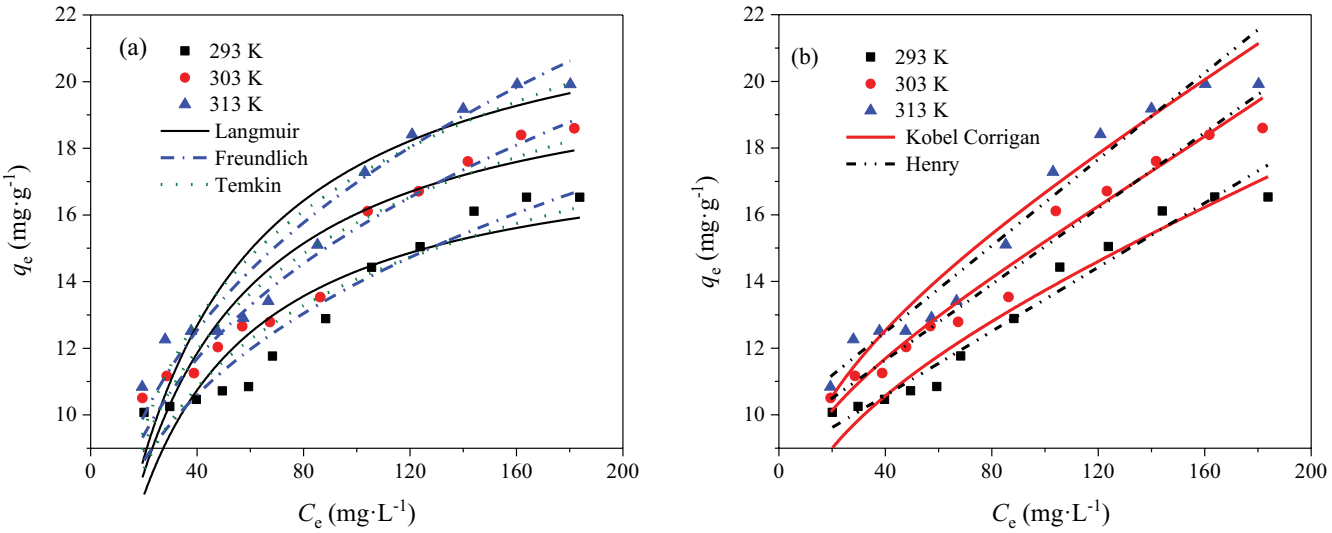

Fig. 4. NGB adsorption isotherms and the non-linear fitted curves of isotherm models at different temperature (CZ dosage 1 g L^{-1}).

If the value of $1/n_F$ is equal to 1, the adsorption is evaluated to linear; if the value of $1/n_F$ is between 0 and 1, the adsorption process is favorable and chemically driven, to some extent. In addition, if $1/n_F$ is above 1, adsorption usually is supposed to be physically driven [30].

Temkin model takes into account the effects of some indirect adsorbent–adsorbate interactions and the fall in the heat of sorption is linear with coverage rather than logarithmic. It is suitable for heterogeneous systems as same as Freundlich isotherm.

Koble–Corrigan model is a combined form of Langmuir and Freundlich expressions [30].

In this study, the nonlinear regressive analysis is performed according to less sum of square of difference of errors. The fitted curves for the adsorption of NGB on CZ are also presented in Fig. 4 and the fitting results of these models are listed in Table 2.

For Langmuir parameters, the calculated maximum adsorption capacity given was 18.4, 21.0, 23.3 mg g^{-1}, respectively at 293, 303, 313 K. They were relatively close to experimental values. Nevertheless, the low coefficients of correlation (R^2) and high values of SSE indicated poor fitting results for Langmuir model. But, at least, the declining K_L with increasing temperature showed the dependence of temperature for adsorption. The low R^2 may be caused by the heterogeneity of modified zeolite. That was to say, the strength of the bond created between the surface of adsorbent and adsorbate were not the same for all sites. Compared with natural zeolite (maximum adsorption capacity 0.940 mg g^{-1} at 303 K), the CPC significantly improved the adsorption capacity for anionic dye through modification of NZ.

Simultaneously, Freundlich model was more suitable for depicting the adsorption process than Langmuir model based on higher R^2 and lower SSE. The important parameter K_F increased with the increasing temperature, inferring that the process be endothermic in nature. In addition, the increasing $1/n_F$ values with the increase of temperature evaluated the decaying trend of adsorption intensity and decreasing heterogeneity on adsorbent surface. From Table 2, the values of $1/n_F$ are between 0.299 and 0.331 and this shows that the adsorption was favorable, chemically driven, and more heterogeneous due to $1/n_F$ near 0. The fitting results agreed with the works carried out by previous researchers which reported that the Freundlich model seemed to provide the best fit with the experimental data for the removal of RR-239 and RB-250 anionic dyes on hexamethylenediamine modified zeolite [14]. That may be related to specific structure of zeolite and surface function groups.

For Temkin model, the A (B) gradually decreased (increased) with the temperature increasing. The R^2 values were below 0.900 and error values were relatively higher, suggesting that the Temkin model was not favorable to depict the adsorption process. Of course, it also indicated that fall in the heat of adsorption was not linear with coverage.

Usually, Henry model was used to depict the gas adsorption. However, if a solid–liquid adsorption process was well depicted by it, it indicated that the coverage of adsorbate on surface of adsorbent was low. From adsorption capacity of this system, the q_m was about 20.0 mg g^{-1}, which was relatively lower.

Finally, the Koble–Corrigan model fitted well from experimental data and curve. The three parameters (A, B, n) showed irregular change and the R^2, SSE were favorable. This result can be deemed that the adsorption process involved in homogeneous and heterogeneous mechanism.

As there were large values of R^2 and smaller values of SSE from Henry model and the fitted curves from Henry model were closer to experimental points, Henry model was best to describe the equilibrium process. The adsorption process is complex from the analysis of fitted results, which may involve in chemical adsorption and endothermic process. The surface of adsorbent exists in low coverage. The adsorption sites may be occupied by monolayer NGB molecular, or the heterogeneous adsorption process may be also take place. From the fitting results, the heterogeneous adsorption should dominate.

Table 1
Expression of isotherm and kinetic models [30,31]

Adsorption modes	Nonlinear expressions	Parameters
Isotherm models		
Langmuir	$q_e = \frac{q_m K_L C_E}{1 + K_L C_E}$	q_m, K_L
Freundlich	$q_e = K_F C_e^{1/n_F}$	K_F, $^{1/n_F}$
Temkin	$q_e = A + B\ln C_e$	A, B
Redlich–Peterson	$q_e = \frac{AC_e}{1 + BC_e^g}$	A, B, g
Koble–Corrigan	$q_e = \frac{AC_e^n}{1 + BC_e^n}$	A, B, n
Henry	$q_e = A + KC_e$	A, K
Kinetic models		
Pseudo-first-order	$q_t = q_t\left(1e - ^{-k_1 t}\right)$	q_e, $k1$
Pseudo-second-order	$q_t = \frac{k_2 q_e^2 t}{1 + k_2 q_e t}$	q_e, $k2$
Elovich	$q_t = \frac{\ln(a\beta)}{\beta} + \frac{\ln t}{\beta}$	a, β
Double constant	$q_t = Ae^{K_s}$	A, K_s
Intraparticle diffusion	$q_t = K_t t^{1/2} + C$	K_t, C

3.2.3. Adsorption kinetic and application of kinetic model

The effect of contact time on adsorption quantity is shown in Fig. 5 for various initial concentrations at three temperatures.

It was seen from Fig. 5 that the whole process was evidently divided by three sections: (1) an initial rapid stage where adsorption rate was fast, (2) a slower second stage where adsorption rate became lower, and (3) a slowest equilibrium adsorption stage.

In order to know deeply adsorption nature, various theories are proposed for describing the kinetics of adsorption for liquid-solid phase systems. These kinetic equations could be classified in two groups namely the adsorption reaction and diffusion models. The former include zero, first, second, third, pseudo-first and pseudo-second-order, and Elovich models, and the latter contain external mass transfer and intra-particle diffusion [31]. In this study, five kinetic models, containing pseudo-first-order, pseudo-second-order, Elovich, double constant and intra-particle diffusion models are selected to investigate the adsorption mechanism.

After fitting the kinetic data using nonlinear regressive analysis according to expression of kinetic models, the values of rate coefficient, determined coefficient R^2, and other parameters are given in Table 3 and the fitted curves are also presented in Fig. 5. Firstly, for pseudo-first-order model, the R^2 values were slightly small, which were almost below 0.900 for initial concentration of 30–60 mg L^{-1} at three temperatures. The SSE was relatively high compared with other models. Moreover, the values of $q_{e(cal)}$ (calculated data from model) were less than values of $q_{e(exp)}$ (obtained from experimental data) in all concentration and temperature scale, which may be attributed to a time lag due to boundary layer or external resistance controlling at the initial stage of sorption [32]. That indicated that the uptake of NGB on CZ was not a first-order reaction.

At all initial concentrations, R^2 values for pseudo-second-order model, which represented the fitting degree between experimental data and theoretical data, were found to be relatively high (almost above 0.900) than pseudo-first-order model. In addition, it can be seen that the difference of $q_{e(cal)}$ and $q_{e(exp)}$ was negligible. Of course, SSE values were also rather small. These results suggested that the NGB adsorption onto CZ may obey to the pseudo-second-order model. The appropriate fit to the pseudo-second-order kinetic model indicated that the adsorption mechanism might depend on both the adsorbate and the adsorbent, and the rate limiting step may be chemisorption involving valence forces through the sharing or exchange of electrons.

According to pseudo-first and pseudo-second-order models, the temperature and initial concentration can all make an effect on rate constant. From Table 3 it is observed that the increasing initial concentration contributed to reducing of k_1 and k_2 at 293 K and 313 K, respectively. But at 303 K, the two rate constants increased firstly and then decreased. Simultaneously, the rate constants varied irregularly at same initial concentration or different temperature. The complex relationship between initial dye concentration or temperature and rate constants suggested that adsorption mechanisms may combine chelation, ion exchange, and physical adsorption.

The adsorption rate is usually controlled by following stages: diffusion from the bulk solution to particle's film surface (boundary layer diffusion); the solute attaches to particle surface through film layer; the solute binds adsorption sites including physic or chemical interaction, ion exchange or complexation. Hence, Weber intra-particle diffusion equation may consist of multi-part (different K_t) representing different adsorption stages. Then, it could be seen from Fig. 5d that diffusion can be part in three regions: external mass surface adsorption (the first sharp section before 120 min); gradual section between 120 min and 360 min; equilibrium stage after 360 min.

Generally, when adsorption steps are not dependent of one another; the plot of q_t against $t_{1/2}$ should give two or more intercepting lines depending on the actual mechanism. Generally, the constant C is proportional to the boundary layer thickness, so the larger C represents greater resistance of boundary layer [33]. According to Table 3 and Fig. 5d, the constants C were not equal to zero and the nonlinear regressive curve did not pass through the origin, indicating that intra-particle diffusion was not sole rate limiting step. This indicated that the intraparticle diffusion was involved in the adsorption process but not the only rate-controlling

Table 2
Parameters of NGB adsorption isotherm models and errors at different temperature

T (K)	293	303	313
		Langmuir	
$q_{m(\text{theo})}$ (mg g^{-1})	18.4 ± 1.3	21.0 ± 1.4	23.3 ± 1.7
K_L (L mg^{-1})	0.0351 ± 0.0093	0.0325 ± 0.0074	0.0298 ± 0.0071
R^2	0.746	0.818	0.814
$q_{e(\text{exp})}$ (mg g^{-1})	16.5	18.6	20.0
SSE	18.8	18.0	24.1
		Freundlich	
K_F	3.52 ± 0.55	3.65 ± 0.45	3.70 ± 0.56
$1/n_F$	0.299 ± 0.380	0.315 ± 0.270	0.331 ± 0.300
R^2	0.882	0.931	0.910
SSE	8.72	6.80	11.7
		Temkin	
A	–2.26 ± 2.08	–3.44 ± 1.94	–4.62 ± 2.38
B	3.55 ± 0.48	4.17 ± 0.45	4.73 ± 0.55
R^2	0.831	0.886	0.868
SSE	12.4	11.3	17.1
		Henry	
A	8.66 ± 0.43	9.36 ± 0.37	9.89 ± 0.57
K	0.0481 ± 0.0041	0.0569 ± 0.0036	0.0648 ± 0.0057
R^2	0.924	0.957	0.922
SSE	5.60	4.24	10.1
		Koble–Corrigan	
A	$7.08 \times 10^{-6} \pm 0.0366$	–14.5 ± 61.1	$5.65 \times 10^{-6} \pm 0.04$
B	–1.00 ± 25.82	–3.05 ± 7.90	–1.00 ± 33.14
n	$1.69 \times 10^{-7} \pm 3.96 \times 10^{-8}$	–0.161 ± 0.418	$1.22 \times 10^{-7} \pm 2.32 \times 10^{-8}$
R^2	0.899	0.949	0.914
SSE	6.73	4.52	10.0

Note: SSE = $\sum_{i=1}^{n}\left(q_c - q_e\right)_i^2$, n is number of experimental points.

step. In another words, some other mechanisms such as complexation or ion-exchange may also control the rate of adsorption.

The Elovich model is related to ion exchange and dramatic change of the activation energy in adsorption process. The parameter a is the initial adsorption rate (mg g^{-1} min^{-1}) while β is the constant relating to fraction of the surface covered and chemisorption activation energy (g mg^{-1}). The fitting data showed the value of a increased with the increase of dye initial concentration while β decreased. Based on the high extremely R^2 and low enough SSE, the adsorption distinctly obeyed to Elovich model, indicating the ion exchange mechanism may be involved in adsorption. Finally, as same as Elovich, double constant equation also made an appropriate depiction.

Based on the observations of the current study, it was conclusion that adsorption kinetic can obey to pseudo-second-order, Elovich, double constant models. It was further confirmed that the fitted curves from these models are closer to experimental points. The intra-particle diffusion is not rate-limiting step and it needs further investigation that whether external mass transfer is rate-limiting step or not.

Similarly, the pH_{pzc} of CZ-NGB was also measured using the aforementioned method. The pH_{pzc} = 5.1 of CZ-NGB was less compared to the pH_{pzc} = 6.3 of CZ. Of course, the result was reasonable due to the load of NGB.

3.3. Secondary adsorption of MB on CZ-NGB

3.3.1. Stability of CZ-NGB and point of zero charge of CZ-NGB

Regeneration of saturated adsorbent or reuse of spent adsorbent was vital to estimate the reusability of the adsorbents and to clarify the mechanism of adsorption, or to explore its new application [23,34–37]. After covered by a

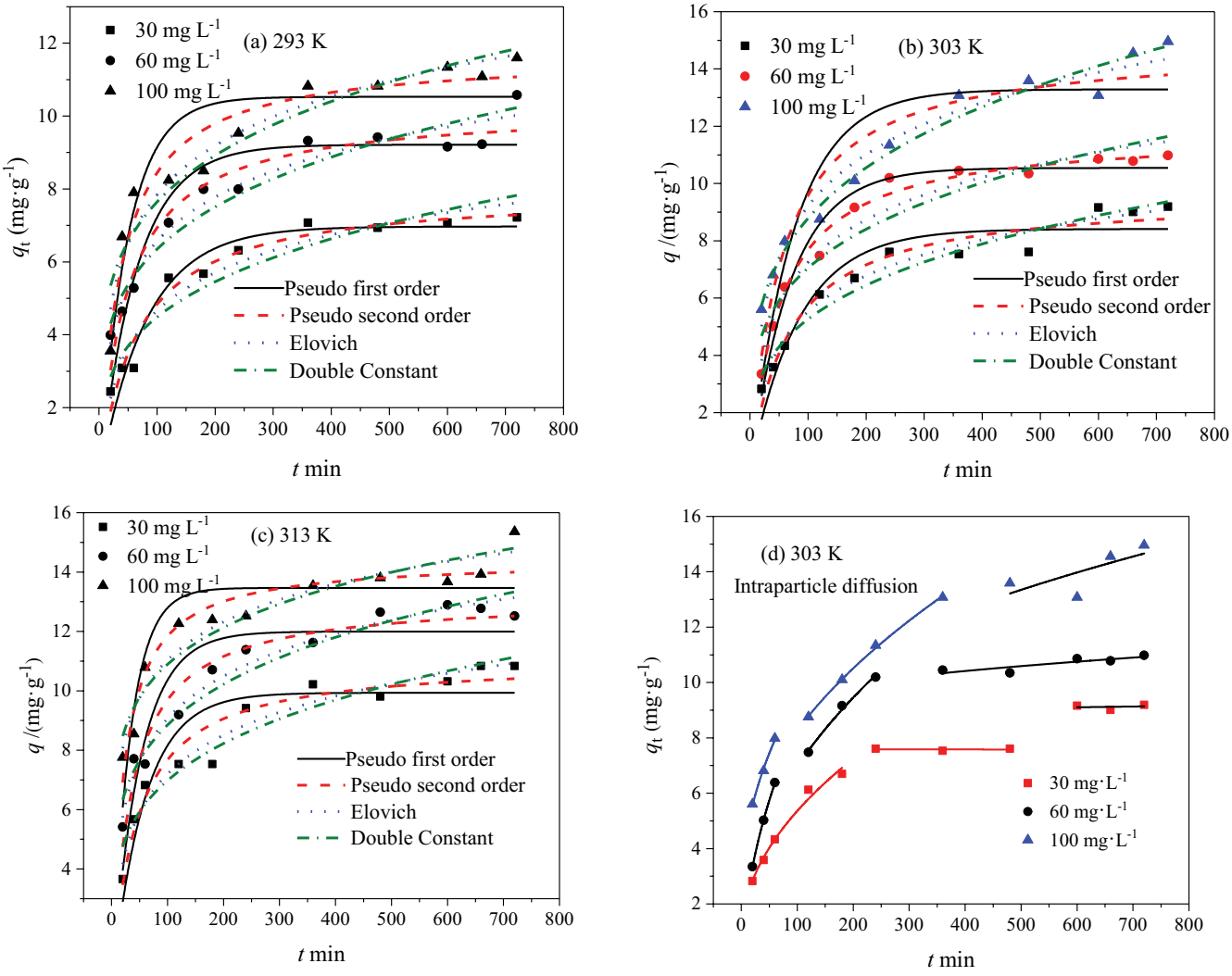

Fig. 5. The fitted curves of five kinetic models for NGB adsorption at 293 K (a), 303 K (b,d), 313 K and (c) (CZ dosage 1 g L^{-1}).

layer of contaminant, the stability of CZ-NGB in various pH conditions was measured. The results showed that NGB was hardly desorbed when pH was below 9.0 (figure not shown). After pH > 9.0, the percent of NGB desorbed from CZ was only below 3%, which was negligible. This indicated the CZ-NGB was enough stable at the whole pH range so that it can be used successfully to further application. Therefore, in next study, the disused or spent CZ loaded by NGB was used as a new adsorbent to adsorb cationic dye MB.

3.3.2. *Effects of pH and salt concentration on adsorption of MB*

Adsorption tests of MB as a function of pH were carried out and the results are shown in Fig. 6a. In Fig. 6a, it was observed that the adsorption quantity changed slightly before pH 7. When pH was above 7, the adsorption quantity rapidly increased until constant value at pH > 9. Similarly, the constant adsorption capacity before pH 7 suggested that the electrostatic mechanism was not the only mechanism for cationic dye adsorption in this system. In addition, when pH was over 7, the surface charges of adsorbent were negative according to pH_{pzc} of CZ-NGB. Thus, the materials were favor to the removal of cationic dye. When pH > 9, the adsorption capacity reached a maximum and kept constant. The optimum pH is obtained at pH > pH_{pzc} from this system. As compared with the adsorption of MB on sunflower oil cake activated carbon reported by Karagöz [38], it got similar conclusion that the optimum pH 6 was over pH_{pzc}. So the solution pH of MB is adjusted to 9.0.

The change of adsorption potential for MB on CZ-NGB with increasing salt concentration is displayed in Fig. 6b. The result clearly demonstrated that the CZ-NGB showed declining ability for MB adsorption in the presence of salt. One factor may be decreasing activity coefficient of dye ions on the condition with higher ionic strength, which limited their transfer to the solid surface [5].

If the adsorption mechanism is main the electrostatic attraction, variations in background electrolyte concentration remarkably influence the adsorbent–adsorbate

Table 3
The kinetic parameters for adsorption of NGB onto CZ

Kinetic model	T (K)								
	293			303			313		
C_0 (mg L^{-1})	30	60	100	30	60	100	30	60	100
Pseudo-first-order									
k_1 (×10^{-2}) (min^{-1})	1.23 ± 0.16	1.53 ± 0.25	2.03 ± 0.35	1.17 ± 0.18	1.40 ± 0.14	1.32 ± 028	1.72 ± 0.34	1.99 ± 0.33	3.00 ± 0.46
$q_{e(theo)}$ (mg g^{-1})	6.97 ± 0.23	9.21 ± 0.35	10.5 ± 0.4	8.41 ± 0.32	10.5 ± 0.2	13.3 ± 0.7	9.93 ± 0.39	12.0 ± 0.4	13.5 ± 0.4
$q_{e(exp)}$ (mg g^{-1})	7.20	10.50	11.50	9.20	11.0	14.9	10.8	12.5	15.3
R^2	0.936	0.851	0.834	0.897	0.955	0.765	0.832	0.824	0.790
SSE	1.81	6.43	9.02	4.69	2.88	22.2	8.44	10.4	10.3
Pseudo-second-order									
k_2 (×10^{-3}) (g mg^{-1} min^{-1})	1.97 ± 0.35	2.05 ± 0.37	2.24 ± 0.41	1.54 ± 0.27	1.59 ± 0.15	1.23 ± 0.30	2.07 ± 0.38	2.15 ± 0.32	3.20 ± 0.52
$q_{e(theo)}$ (mg g^{-1})	7.94 ± 0.29	10.2 ± 0.3	11.7 ± 0.4	9.59 ± 0.33	11.8 ± 0.2	14.8 ± 0.7	11.0 ± 0.3	13.1 ± 0.3	14.4 ± 0.3
R^2	0.958	0.936	0.931	0.955	0.986	0.898	0.937	0.947	0.918
SSE	1.19	2.73	3.74	2.03	0.925	9.70	3.19	3.13	4.03
Elovich									
a (mg g^{-1} min^{-1})	0.336 ± 0.083	0.744 ± 0.177	1.09 ± 0.35	0.384 ± 0.063	0.635 ± 0.138	0.891 ± 0.178	0.852 ± 0.207	1.66 ± 0.38	7.25 ± 3.58
β (g mg^{-1})	0.667 ± 0.057	0.571 ± 0.038	0.514 ± 0.043	0.552 ± 0.031	0.468 ± 0.031	0.383 ± 0.023	0.528 ± 0.035	0.484 ± 0.026	0.541 ± 0.047
R^2	0.938	0.958	0.935	0.970	0.957	0.966	0.958	0.971	0.931
SSE	1.74	1.82	3.52	1.36	2.75	3.19	2.13	1.69	3.40

(Continued)

Table 3 Continued

Kinetic model	T (K)								
	293			303			313		
C_0 (mg L^{-1})	30	60	100	30	60	100	30	60	100
	Double constant								
A	1.22 ± 0.27	2.09 ± 0.28	2.75 ± 0.43	1.37 ± 0.20	2.18 ± 0.40	2.60 ± 0.23	2.35 ± 0.32	3.40 ± 0.35	5.32 ± 0.52
K_s	0.282 ± 0.038	0.242 ± 0.023	0.222 ± 0.027	0.292 ± 0.025	0.254 ± 0.031	0.264 ± 0.015	0.237 ± 0.023	0.208 ± 0.018	0.156 ± 0.017
R^2	0.893	0.937	0.898	0.950	0.900	0.977	0.930	0.946	0.908
SSE	3.02	2.69	5.56	2.28	6.38	2.17	3.53	3.20	4.54
	Intraparticle diffusion								
K_{t1}	0.477 ± 0.113	0.482 ± 0.037	1.35 ± 0.24	0.455 ± 0.033	0.925 ± 0.013	0.724 ± 0.048	0.973 ± 0.078	0.534 ± 0.078	0.731 ± 0.130
C	0.0275± 0.8772	1.69 ± 0.29	–2.27 ± 1.50	0.805 ± 0.301	–0.807± 0.084	2.32 ± 0.31	–0.627 ± 0.491	3.53 ± 0.72	4.45 ± 1.01
R^2	0.848	0.982	0.94	0.98	1	0.991	0.987	0.919	0.910
SSE	0.577	0.0625	0.303	0.167	0.000960	0.0126	0.0325	0.952	0.763
K_{t2}	0.249 ± 0.025	0.253 ± 0.101	0.338 ± 0.051	0.000578 ± 0.013740	0.600 ± 0.052	0.542 ± 0.014	0.374 ± 0.101	0.193 ± 0.080	0.216 ± 0.062
C	2.37 ± 0.40	4.39 ± 1.62	4.30 ± 0.77	7.59 ± 0.26	0.965 ± 0.706	2.85 ± 0.21	3.17 ± 1.52	8.25 ± 1.51	9.37 ± 1.00
R^2	0.981	0.727	0.934	–0.996	0.985	0.998	0.808	0.710	0.849
SSE	0.00958	0.160	0.182	0.00390	0.0286	0.0130	0.708	0.131	0.0601
K_{t3}	0.0574 ± 0.0023	0.174 ± 0.186	0.131 ± 0.062	0.0141 ± 0.0813	0.075 ± 0.025	0.293 ± 0.201	0.228 ± 0.040	–0.159 ± 0.034	0.255 ± 0.192
C	5.68 ± 0.06	5.29 ± 4.60	7.96 ± 1.54	8.76 ± 2.09	8.92 ± 0.60	6.79 ± 4.98	4.82 ± 0.99	16.8 ± 0.9	7.89 ± 4.77
R^2	0.997	–0.0428	0.535	–0.942	0.664	0.275	0.913	0.913	0.201
SSE	0.0000661	0.921	0.103	0.0181	0.0754	1.08	0.0426	0.00313	0.987

interactions. The effects of ionic strength verified that the adsorption mechanism involve the electrostatic interaction in this system.

3.3.3. Adsorption equilibrium studies

Fig. 7 shows the adsorption isotherms of MB adsorption onto CZ-NGB at different temperatures. It was clearly seen from Fig. 7 that it was in favor of adsorption at higher temperature and the MB adsorption was also endothermic.

It was also observed from Fig. 7 that the experimental adsorption capacity of MB on CZ-NGB were 9.22, 11.8, 18.4 mg g^{-1} from 293 K to 313 K, respectively. The adsorption capacity of MB on natural zeolite was 19.3 mg g^{-1} at 303 K, indicating that the adsorption of MB on CZ-NGB was lower. But it was still available for practical application.

Redlich–Peterson model which contains three parameters had been proposed in order to overcome the limitation of Langmuir and Freundlich models. It can be applied to either in homogeneous or heterogeneous systems due to its versatility. The Redlich–Peterson constant g (usually $0 < g < 1$), which represents the degree of heterogeneity, can be used to evaluated whether adsorption process favorable or not. There are two limited boundary situation: when $g = 0$, the equation is simplified to Henry equation, which means the low surface coverage on adsorbent. And this situation may take place on the condition of low initial adsorbate concentration; Nevertheless, when $g = 1$, the equation obviously transfer into Langmuir isotherm [31].

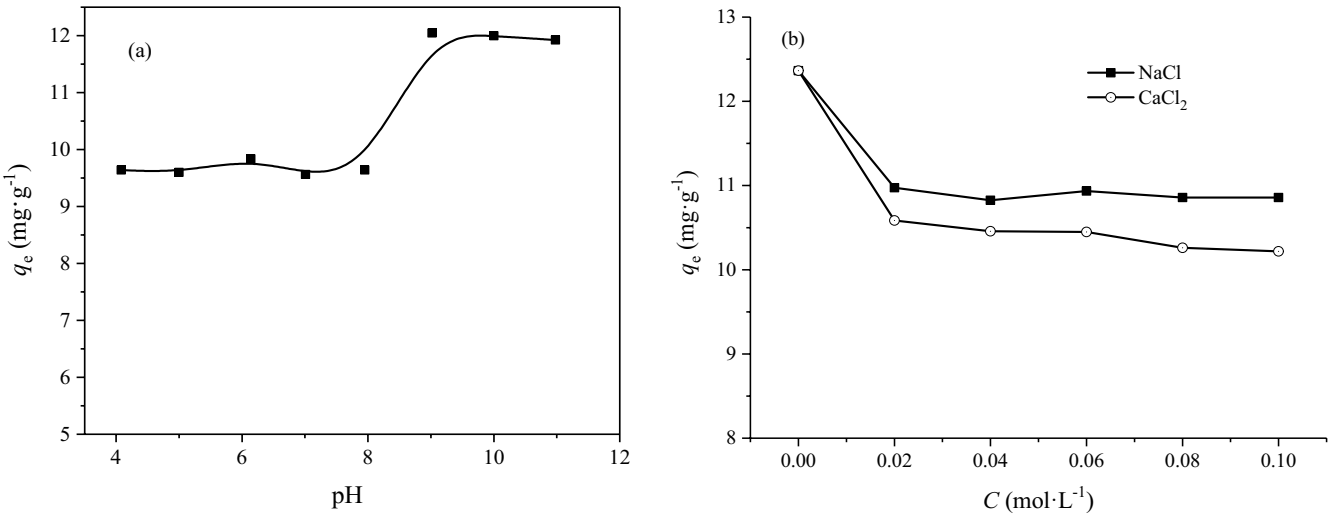

Fig. 6. (a) Effect of pH on adsorption capacity of MB on CZ-NGB and (b) Effect of salt concentration on adsorption capacity of MB on CZ-NGB (C_0 = 30 mg L^{-1}, CZ-NGB dosage 1 g L^{-1}, t = 720 min, T = 303 K).

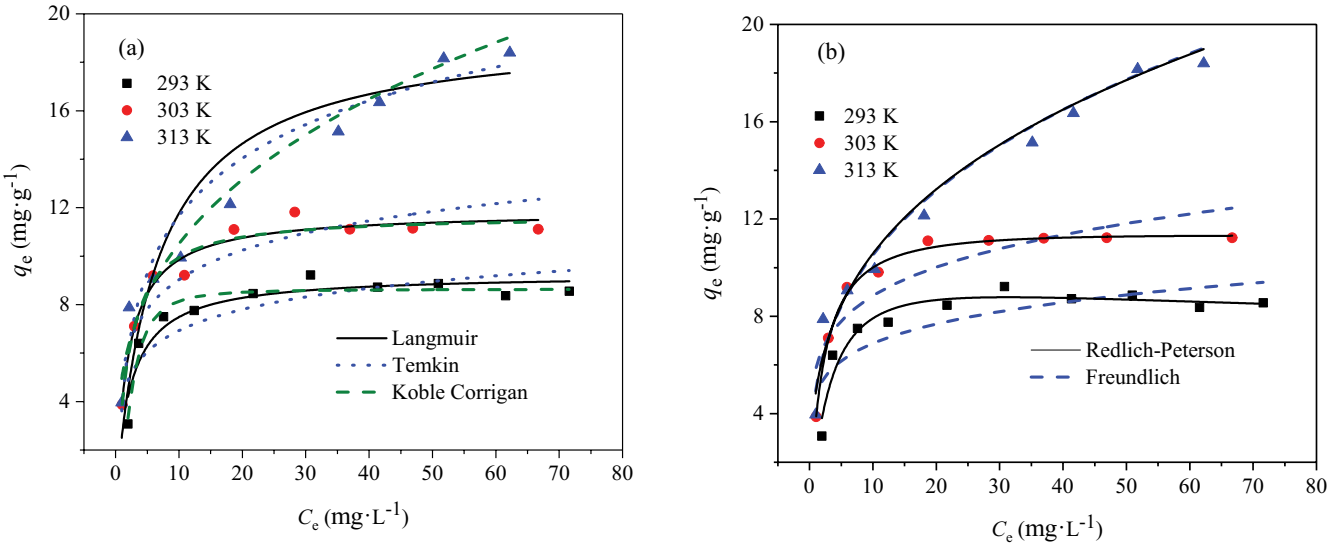

Fig. 7. MB adsorption isotherm curves and the non-linear fitted curves of isotherm models at different temperature (CZ-NGB dosage 1 g L^{-1}).

According to the experimental data, the five models, containing Langmuir, Freundlich, Temkin, Redlich–Peterson, and Koble–Corrigan models are used to evaluate the isotherm. The fitted curves are also presented in Fig. 7 and these fitting results are listed in Table 4.

As a whole, Redlich–Peterson and Koble–Corrigan models seemed to more favorable than other models on the ground of higher R^2 (nearly above 0.950) and lower SSE in the whole temperature range. Langmuir model seemed to be more suitable for lower temperature while Freundlich model and Temkin model showed better fitting parameters at higher temperature. Those deduced that monolayer adsorption was mainly mechanism at lower temperature while the multilayer adsorption gradually dominated with the increase of temperature.

In addition, the $1/n_F$ of Freundlich model declined with increase of temperature, and the values were less than 1. So the adsorption was favorable. It may be attributed that the multilayer adsorption behavior made a fierce competition between adsorbate molecules.

In Redlich–Peterson model, the value of A and B increased with increasing temperature, but the g value decreased from above 1 to below 1. At 293 K and 303 K, the g value approach to 1, which showed the expression of equation was closed to Langmuir model.

Finally, the Koble–Corrigan model was also applied to homogeneous or heterogeneous systems as same as Redlich–Peterson model. Its excellent fitting result showed the complexity of adsorption process. The value of n also decreased with increasing temperature in accordance with g value of Redlich–Peterson model.

According to the above nonlinear regression results, it was concluded that Redlich–Peterson and Koble–Corrigan models be successfully used to depict the adsorption of MB on CZ-NGB. In addition, the uptake was more suitable for Langmuir model at lower temperature while Freundlich model at higher temperature, so the adsorption process was deemed to relate to homogeneous and heterogeneous uptake on the different conditions.

Table 4
Parameters of MB adsorption isotherm models and errors at different temperature

T (K)	293	303	313
Langmuir			
$q_{m(\text{theo})}$ (mg g^{-1})	9.26 ± 0.31	11.8 ± 0.3	19.4 ± 1.6
K_L (L mg^{-1})	0.423 ± 0.088	0.494 ± 0.068	0.155 ± 0.053
R^2	0.889	0.962	0.866
$q_{e(\text{exp})}$ (mg g^{-1})	9.22	11.8	18.4
SSE	2.92	1.76	25.8
Freundlich			
K_F	4.78 ± 0.72	5.84 ± 0.74	4.99 ± 0.54
$1/n_F$	0.158 ± 1.740	0.180 ± 1.200	0.323 ± 0.290
R^2	0.643	0.778	0.958
SSE	9.39	10.4	8.17
Temkin			
A	4.02 ± 0.82	5.00 ± 0.72	3.76 ± 0.98
B	1.26 ± 0.26	1.75 ± 0.25	3.43 ± 0.34
R^2	0.715	0.86	0.928
SSE	7.49	6.56	14
Redlich–Peterson			
A	2.71 ± 0.55	5.22 ± 1.06	89.4 ± 739.6
B	0.186 ± 0.082	0.393 ± 0.145	17.3 ± 148.6
g	1.12 ± 0.06	1.03 ± 0.05	0.685 ± 0.078
R^2	0.919	0.959	0.951
SSE	1.85	1.64	8.15
Koble–Corrigan			
A	1.40 ± 0.56	5.50 ± 1.05	4.98 ± 0.81
B	0.161 ± 0.065	0.472 ± 0.086	–0.008 ± 0.242
n	2.01 ± 0.38	1.09 ± 0.19	0.317 ± 0.186
R^2	0.946	0.958	0.951
SSE	1.23	1.69	8.17

3.3.4. Kinetic analysis

Fig. 8 is the kinetic curve about MB adsorption onto CZ-NGB. The trend of curves was similar to NGB adsorption onto CZ.

Four kinetic models are selected to fit the kinetic data for obtaining most appropriate equation and the results are presented in Fig. 8 (fitted curves) and Table 5 (related parameters), respectively.

In terms of pseudo-first and pseudo-second-order models, the R^2 and residual sum of squares were all not satisfactory, especially R^2 which almost all low 0.800. Furthermore, the values of $q_{e(\text{cal})}$ were over the vales of $q_{e(\text{exp})}$ in all concentration and temperature scale for pseudo-first-order model, which may be attributed to a time lag as same as NGB adsorption on CZ. Similarly, the disordered change trend of rate constant k_1 and k_2 with initial concentration and temperature suggested the complex mechanism about secondary adsorption.

In this system, the intra-particle diffusion model was used to fit whole curve rather than piece-wise curve. The result showed this model could be able to depict successfully adsorption. The higher initial MB concentration, the larger diffusion rate constant K_t. This reason may be that the increase of initial concentration enhanced concentration gradient between bulk solution and surface of adsorbent. In addition, the C value was above zero, suggesting the intra-particle diffusion model could not fully control diffusion process. The C value also enhanced with increasing initial concentration except at 318 K. So the effect of boundary layer would larger and larger on the above condition.

The change trend of the parameter A from double constant model was in accordance with K_t in intra-particle diffusion model. From R^2 and SSE analysis, the double constant and intraparticle diffusion models was appropriate to predict the secondary adsorption, but Elovich model seemed to be not suitable, which indicated the ion exchange may be not mainly mechanism.

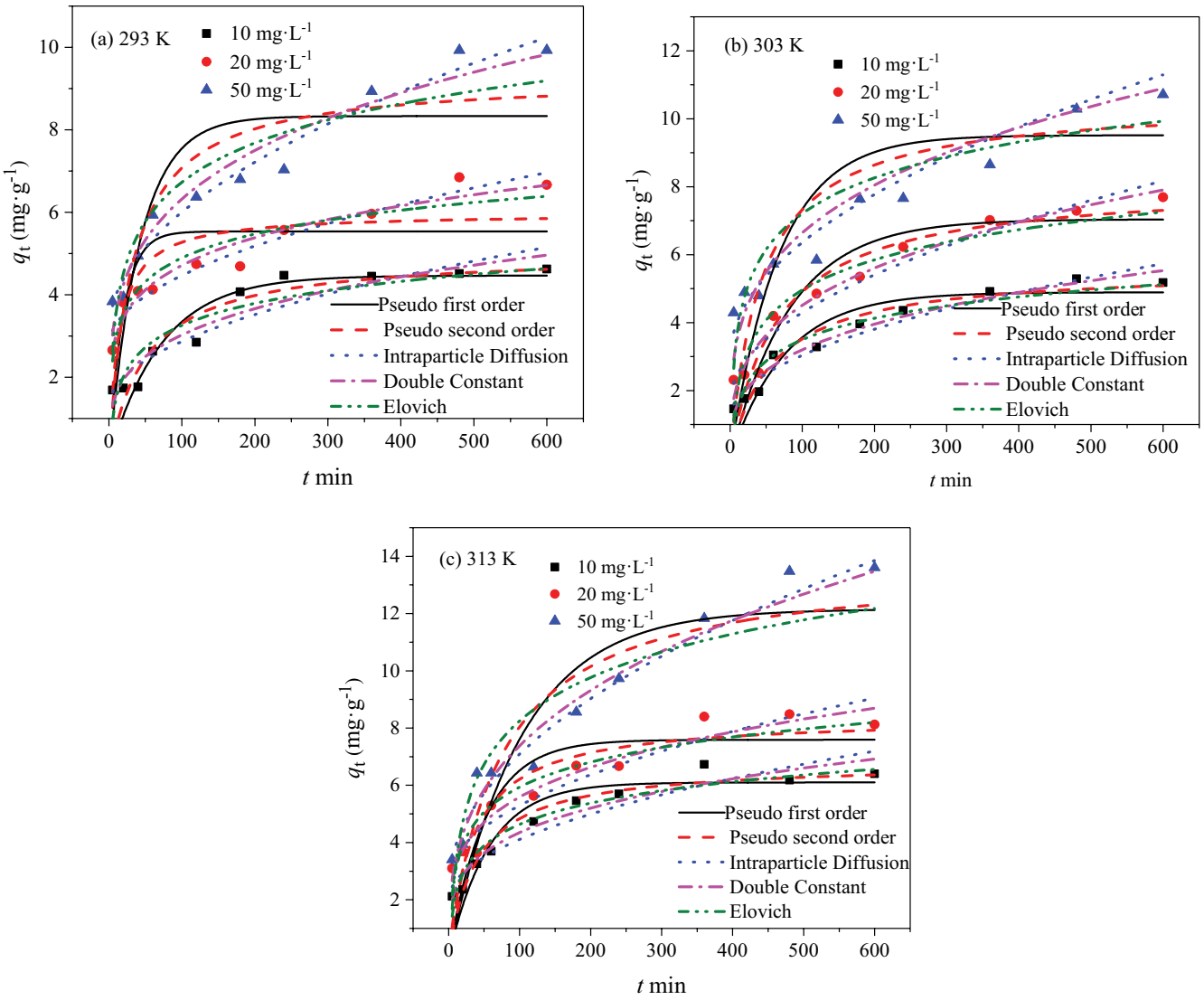

Fig. 8. The fitted curves of five kinetic models for MB adsorption at 293 K (a), 303 K (b,d), 313 K and (c) (CZ-NGB dosage 1 g L^{-1}).

Yan reported the secondary adsorption of methyl orange onto MB-loaded carboxymethyl cellulose, concluding that electrostatic adsorption may be mainly mechanism rather than ion exchange [24]. The result was similar to this study. Liu studied the secondary adsorption of Congo red onto MB-loaded magnetic grapheme oxide composites [39]. Compared to direct adsorption, the adsorption capacity was improved, and the exhausted adsorbent can be utilized again. Electrostatic adsorption and hydrophobic interaction were main mechanism.

3.4. Supposal of adsorption mechanisms

Based on the afore mentioned investigation, it can be concluded that the adsorption of NGB onto CZ with CPC layer coverage may contain the following mechanism: (1) electrostatic attraction between anionic dye and CPC molecule with positive charge's head group; (2) ion exchange between anionic dye molecule and Cl^- from CPC; (3) hydrophobic interaction between the hydrophobic tails of CPC layer and the hydrophobic functional groups of NGB; (4) Van der Waals' force [40–43].

In CPC modification process, when the CPC concentration exceeds the specific concentration in aqueous solution, the CPC^+ adhered to the zeolite surface can aggregate to form structural bilayer or admicelles. Generally, the large molecule CPC only could cover the external surface and not enter the smaller pores on zeolite surface to displace the Na^+ [44], which decreased the surface area of natural zeolite. In addition, the optimum concentration of CPC was explored. As a result, 3% CPC as optimum concentration was supposed to the bilayer coverage of surfactant. Then, bilayer CPC formation bring about charge reversal on the external surface of zeolite from negative to positive and the positively charged head groups of CPC are balanced by counter-ions chloride [45].

Table 5
The kinetic parameters for adsorption of MB onto CZ-NGB

Kinetic model	MB onto CZ-NGB								
	293 K			303 K			313 K		
C_0 (mg L^{-1})	10	20	50	10	20	50	10	20	50
Pseudo-first-order									
k_1 (×10^{-2}) (min^{-1})	1.38 ± 0.37	5.16 ± 2.09	2.36 ± 0.86	1.30 ± 0.30	1.20 ± 0.30	1.48 ± 0.63	1.76 ± 0.39	1.96 ± 0.60	9.83 ± 0.32
$q_{e(theo)}$ (mg g^{-1})	4.47 ± 0.32	5.54 ± 0.40	8.33 ± 0.71	4.89 ± 0.32	7.04 ± 0.50	9.51 ± 1.08	6.10 ± 0.34	7.60 ± 0.57	12.2 ± 1.2
$q_{e(exp)}$ (mg g^{-1})	4.6	6.6	9.3	5.2	7.7	10.7	6.4	8.4	13.6
R^2	0.765	0.409	0.493	0.832	0.807	0.353	0.821	0.641	0.703
SSE	3.04	8.42	20.5	2.80	6.64	36.3	4.13	11.9	30.6
Pseudo-second-order									
k_2 (×10^{-3}) (g mg^{-1} min^{-1})	3.84 ± 1.61	12.6 ± 5.8	3.47 ± 1.72	3.06 ± 0.99	1.90 ± 0.70	2.17 ± 1.36	3.65 ± 1.12	3.42 ± 1.44	1.02 ± 0.48
$q_{e(theo)}$ mg g^{-1})	5.02 ± 0.43	5.98 ± 0.39	9.27 ± 0.81	5.58 ± 0.38	8.10 ± 0.65	10.5 ± 1.3	6.78 ± 0.40	8.38 ± 0.65	13.8 ± 1.4
R^2	0.812	0.664	0.673	0.897	0.87	0.543	0.889	0.769	0.805
SSE	2.43	4.79	13.2	1.72	4.48	25.6	2.58	7.66	20.2
Intraparticle diffusion									
K_t	0.157 ± 0.020	0.172 ± 0.013	0.293 ± 0.018	0.186 ± 0.015	0.267 ± 0.020	0.340 ± 0.028	0.213 ± 0.025	0.259 ± 0.025	0.467 ± 0.029
C	1.29 ± 0.30	2.75 ± 0.19	3.08 ± 0.26	1.18 ± 0.22	1.62 ± 0.30	2.95 ± 0.40	1.98 ± 0.36	2.70 ± 0.37	2.42 ± 0.42
R^2	0.867	0.948	0.967	0.943	0.95	0.943	0.890	0.920	0.967
SSE	1.72	0.743	1.33	0.946	1.71	3.2	2.55	2.65	3.39

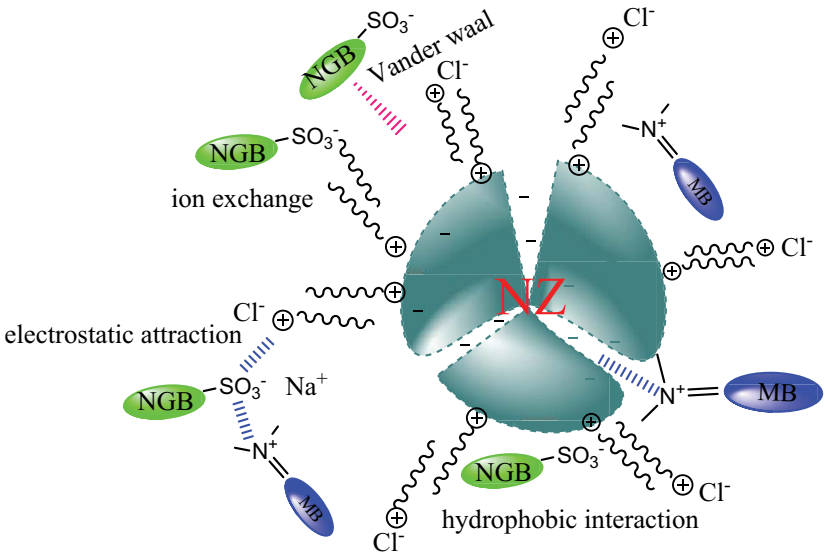

Fig. 9. Mechanisms of NGB adsorption on CZ and MB adsorption on CZ-NGB.

Thus, if the supposal that bilayer coverage of surfactant was reasonable, the electrostatic attraction should be included in adsorption mechanism. The results of effects of pH and ion strength on NGB adsorption had supported this point. In particular, the $-SO_3^-$ group from NGB molecules showed strong attraction with positively charged head groups of CPC.

Of course, beside electrostatic attraction, the hydrophobic interaction was also taken into account as the specific structure of surfactant [46]. The existence of hydrophobic group of anionic dye made NGB enter easily into CPC layer. In addition, as is known to us, the Van der Waal's force also exist between adsorbent and dye. Cationic surfactant modified walnut shell or Phoenix tree leaf can also bind neutral molecule such as Bisphenol A or 2,4-dichlorophenol through hydrophobic interaction and hydrogen bond [47,48]. The interaction between CZ and NGB is showed in Fig. 9.

The adsorption of MB on CZ-NGB is more complex than NGB on CZ. First of all, in terms of the purpose of this study, the cationic MB was expected to be bonded by anionic NGB through electrostatic attraction. According to investigation about effects of pH and ion strength on MB adsorption, the electrostatic attraction was surely one of mechanisms of secondary adsorption.

The adsorption capacity of NGB on CZ was observed to be not higher. In other words, the load ratio of NGB on CZ was lower. Then, the layer of bare CZ may also bond MB by hydrophobic interaction. Even, there exists still a small fraction of surface of natural zeolite which not be covered by CPC. The negatively charged bare surface of NZ would attract the cationic MB molecules. The interaction between MB and CZ-NGB is also shown in Fig. 9.

4. Conclusion

In this paper, the zeolite surface was covered by CPC with positive charges, increasing interaction between metal complex dye with negative charges and the zeolite surfaces. The CPC bonded successfully on the surface of NZ. Lower pH and higher ions strength could be able to enhance the adsorption capacity of NGB on CZ. The adsorption of NGB on CZ had temperature dependence. The adsorption isotherms closely followed Freundlich, Henry, Koble–Corrigan models. The adsorption kinetics was better fitted by pseudo-second-order, Elovich, double constant models. Then, the disused adsorbent was hopeful as a new adsorbent in secondary adsorption due to an altered surface structure. Higher pH and lower ionic strength were benefit with MB adsorption on CZ-NGB. Adsorption isotherm was best fitted by Redlich–Peterson and Koble–Corrigan while the kinetics was well described by both intraparticle diffusion and double constant models. From the discussion mechanism for CZ on NGB and secondary adsorption, it was conclusion that several interaction existed between adsorbent and dye: electrostatic attraction, ion exchange, hydrophobic interaction and Van der Waals' force. Modified zeolite is promising to effectively bind some dyes from solution. Future study is focused on utilization of CZ to remove selected dyes from real wastewater.

Acknowledgements

This work was financially supported by the Henan province basis and advancing technology research project (142300410224).

References

[1] G. Crini, E. Lichtfouse, Advantages and disadvantages of techniques used for wastewater treatment, Environ. Chem. Lett., 7 (2018) 45–155.
[2] A.A. Aryee, F.M. Mpatani, A.N. Kani, E. Dovi, R.P. Han, Z.H. Li, L.B. Qu, A review on functionalized adsorbents based on peanut husk for the sequestration of pollutants in wastewater: modification methods and adsorption study, J. Clean. Prod., 310 (2021) 127502, doi: 10.1016/j.jclepro.2021.127502.

[3] Z. Aksu, G. Karabayir, Comparison of biosorption properties of different kinds of fungi for the removal of Gryfalan Black RL metal-complex dye, Bioresour. Technol., 99 (2008) 7730–7741.
[4] A. Masafumi, T. Bredow, K. Jug, What is the origin of color on metal complex dyes? Theoretical analysis of a Ni-coordinate azo dye, Dyes Pigm., 63 (2004) 225–230.
[5] A. Kumar, G. Sharma, Mu. Naushad, A.H. Al-Muhtaseb, A. García-Peñas, G.T. Mola, CL. Si, F.J. Stadler, Bio-inspired and biomaterials-based hybrid photocatalysts for environmental detoxification: a review, Chem. Eng. J., 382 (2020) 122937, doi: 10.1016/j.cej.2019.122937.
[6] F.M. Mpatani, R.P. Han, A.A. Aryee, A.N. Kani, Z.H. Li, L.B. Qu, Adsorption performance of modified agricultural waste materials for removal of emerging micro-contaminant bisphenol A: a comprehensive review, Sci. Total Environ., 780 (2021) 146629, doi: 10.1016/j.scitotenv.2021.146629.
[7] S. Samsami, M. Mohamadizaniani, M.H. Sarrafzadeh, E.R. Rene, M. Firoozbahr, Recent advances in the treatment of dye-containing wastewater from textile industries: overview and perspectives, Process Saf. Environ. Prot., 143 (2020) 138–163.
[8] G. Crini, E. Lichtfouse, L.D. Wilson, N. Morin-Crini, Conventional and non-conventional adsorbents for wastewater treatment, Environ. Chem. Lett., 17 (2019) 195–1213.
[9] S.B. Wang, Y.L. Peng, Natural zeolites as effective adsorbents in water and wastewater treatment, Chem. Eng. J., 156 (2010) 11–24.
[10] V. Hernández-Montoya, M.A. Pérez-Cruz, D.I. Mendoza-Castillo, M.R. Moreno-Virgen, A. Bonilla-Petriciolet, Competitive adsorption of dyes and heavy metals on zeolitic structures, J. Environ. Manage., 116 (2013) 213–221.
[11] R.P. Han, J.J. Zhang, P. Han, Y.F. Wang, Z.H. Zhao, M.S. Tang, Study of equilibrium, kinetic and thermodynamic parameters about Methylene blue adsorption onto natural zeolite, Chem. Eng. J., 145 (2009) 496–504.
[12] R.P. Han, Y. Wang, Q. Sun, L.L. Wang, J.Y. Song, X.T. He, C.C. Dou, Malachite green adsorption onto natural zeolite and reuse by microwave irradiation, J. Hazard. Mater., 175 (2010) 1056–1061.
[13] D. Karadag, Modeling the mechanism, equilibrium and kinetics for the adsorption of Acid Orange 8 onto surfactant-modified clinoptilolite: the application of nonlinear regression analysis, Dyes Pigm., 74 (2007) 659–664.
[14] T. Zhou, W.Z. Lu, L.F. Liu, H.M. Zhu, Y.B. Jiao, S.S. Zhang, R.P. Han, Effective adsorption of light green anionic dye from solution by CPB modified peanut in column mode, J. Mol. Liq., 211 (2015) 909–2914.
[15] D. Karadag, E. Akgul, S. Tok, F. Erturk, M.A. Kaya, M. Turan, Basic and reactive dye removal using natural and modified zeolites, J. Chem. Eng. Data, 52 (2007) 2436–2441.
[16] R.D. Zhang, X.N. Zhang, C.C. Dou, R.P. Han, Adsorption of congo red from aqueous solutions using cationic surfactant modified wheat straw in batch mode: kinetic and equilibrium study, J. Taiwan Inst. Chem. Eng., 45 (2014) 2578–2583.
[17] C. Lei, Y.Y. Hu, M.Z. He, Adsorption characteristics of triclosan from aqueous solution onto cetylpyridinium bromide (CPB) modified zeolites, Chem. Eng. J., 219 (2013) 361–370.
[18] B.L. Zhao, W. Xiao, Y. Shang, H.M. Zhu, R.P. Han, Adsorption of light green anionic dye using cationic surfactant-modified peanut husk in batch mode, Arabian J. Chem., 10 (2017) S3595–S3602.
[19] B.C. Oei, S. Ibrahim, S.B. Wang, H.M. Ang, Surfactant modified barley straw for removal of acid and reactive dyes from aqueous solution, Bioresour. Technol., 100 (2009) 4292–4295.
[20] Y.Y. Su, B.L. Zhao, W. Xiao, R.P. Han, Adsorption behavior of light green anionic dye using cationic surfactant modified wheat straw in batch and column mode, Environ. Sci. Pollut. Res., 20 (2013) 5558–5568.
[21] S.Y. Lin, W.F. Chen, M.T. Cheng, Q. Li, Investigation of factors that affect cationic surfactant loading on activated carbon and perchlorate adsorption, Colloids Surf., A, 34 (2013) 236–242.
[22] R. Chitrakar, Y. Makita, T. Hirotsu, A. Sonoda, Montmorillonite modified with hexadecylpyridinium chloride as highly efficient anion exchanger for perchlorate ion, Chem. Eng. J., 191 (2012) 141–146.
[23] M.Y. Liu, X.Y. Li, Y.Y. Du, R.P. Han, Adsorption of methyl blue from solution using walnut shell and reuse in a secondary adsorption for Congo red, Bioresour. Technol. Rep., 5 (2019) 238–242.
[24] H. Yan, W.X. Zhang, X.W. Kan, L. Dong, Z.W. Jiang, H.J. Li, H. Yang, R.S. Cheng, Sorption of Methylene blue by carboxymethyl cellulose and reuse process in a secondary sorption, Colloids Surf., A, 380 (2011) 143–151.
[25] R.P. Han, L.N. Zou, X. Zhao, Y.F. Xu, F. Xu, Y.L. Li, Y. Wang, Characterization and properties of iron oxide-coated zeolite as adsorbent for removal of copper(II) from solution in fixed bed column, Chem. Eng. J., 149 (2009) 123–131.
[26] Y.H. Zhan, Z.L. Zhu, J.W. Lin, Y.L. Qiu, J.F. Zhao, Removal of humic acid from aqueous solution by cetylpyridinium bromide modified zeolite, J. Environ. Sci., 22 (2010) 1327–1334.
[27] D.S. Sun, X.D. Zhang, Y.D. Wu, X. Liu, Adsorption of anionic dyes from aqueous solution on fly ash, J. Hazard. Mater., 181 (2010) 335–342.
[28] J.Y. Li, J. Ma, Q.H. Guo, S.L. Zhang, H.Y. Han, S.S. Zhang, R.P. Han, Adsorption of hexavalent chromium from solution using modified walnut shell, Water Sci. Technol., 81 (2020) 824–833.
[29] G. Alberghina, R. Bianchini, M. Fichera, S. Fisichella, Dimerization of Cibacron Blue F3GA and other dyes: influence of salts and temperature, Dyes Pigm., 46 (2000) 129–137.
[30] M. Benjelloun, Y. Miyah, G.A. Evrendilek, F. Zerrouq, S. Lairini, Recent advances in adsorption kinetic models: their application to dye types, Arabian J. Chem., 14 (2021) 103031, doi: 10.1016/j.arabjc.2021.103031.
[31] K.Y. Foo, B.H. Hameed, Insights into the modeling of adsorption isotherm systems, Chem. Eng. J., 156 (2010) 2–10.
[32] H.N. Bhatti, Z. Mahmood, A. Kausar, S.M. Yakout, O.H. Shair, M. Iqbal, Biocomposites of polypyrrole, polyaniline and sodium alginate with cellulosic biomass: adsorption-desorption, kinetics and thermodynamic studies for the removal of 2,4-dichlorophenol, Int. J. Biol. Macromol., 153 (2020) 146–157.
[33] A. Safa Özcan, B. Erdem, A. Özcan, Adsorption of Acid Blue 193 from aqueous solutions onto BTMA-bentonite, Colloids Surf., A, 266 (2005) 73–81.
[34] A.A. Aryee, F.M. Mpatani, Y. Du, A.N. Kani, E. Dovi, R. Han, Z. Li, L. Qu, Fe_3O_4 and iminodiacetic acid modified peanut husk as a novel adsorbent for the uptake of Cu(II) and Pb(II) in aqueous solution: characterization, equilibrium and kinetic study, Environ. Pollut., 268 (2021) 115729, doi: 10.1016/j.envpol.2020.115729.
[35] N.I. Taib, N.A. Rosli, N.I. Saharrudin, N.M. Rozi, N.A.A. Kasdiehram, N.N.T. Abu Nazri, Kinetic, equilibrium, and thermodynamic studies of untreated watermelon peels for removal of copper(II) from aqueous solution, Desal. Water Treat., 227 (2021) 289–299.
[36] J.L. Wang, X. Liu, M.M. Yang, H.Y. Han, S.S. Zhang, G.F. Ouyang, R.P. Han, Removal of tetracycline using modified wheat straw from solution in batch and column modes, J. Mol. Liq., 338 (2021) 116698, doi: 10.1016/j.molliq.2021.116698.
[37] A.A. Aryee, E. Dovi, X.X. Shi, R.P. Han, Z.H. Li, L.B. Qu, Zirconium and iminodiacetic acid modified magnetic peanut husk as a novel adsorbent for the sequestration of phosphates from solution: characterization, equilibrium and kinetic study, Colloids Surf., A, 615 (2021) 126260, doi: 10.1016/j.colsurfa.2021.126260.
[38] S. Karagöz, T. Tay, S. Ucar, M. Erdem, Activated carbons from waste biomass by sulfuric acid activation and their use on Methylene blue adsorption, Bioresour. Technol., 99 (2008) 6214–6222.
[39] M.Y. Liu, J.J. Dong, W.L. Wang, M.M. Yang, Y.F. Gu, R.P. Han, Study of methylene mlue adsorption from solution by magnetic graphene oxide composites, Desal. Water Treat., 147 (2019) 398–408.
[40] J.W. Lin, Y.W. Zhan, Z.L. Zhu, Y.Q. Xing, Adsorption of tannic acid from aqueous solution onto surfactant-modified zeolite, J. Hazard. Mater., 193 (2011) 102–111.

[41] F.M. Mpatani, R.P. Han, A.A. Aryee, A.N. Kani, Z.H. Li, L.B. Qu, Adsorption performance of modified agricultural waste materials for removal of emerging micro-contaminant bisphenol A: a comprehensive review, Sci. Total Environ., 780 (2021) 146629, doi: 10.1016/j.scitotenv.2021.146629.
[42] R. Bushra, S. Mohamad, Y. Alias, Y.C. Jin, M. Ahmad, Current approaches and methodologies to explore the perceptive adsorption mechanism of dyes on low-cost agricultural waste: a review, Microporous Mesoporous Mater., 319 (2021) 111040, doi: 10.1016/j.micromeso.2021.111040.
[43] A.K. Badawi, E.S. Bakhoum, K. Zaher, Sustainable evaluation of using nano zero-valent iron and activated carbon for real textile effluent remediation, Arabian J. Sci. Eng., 46 (2021) 10365–10380.
[44] H.P. Chao, S.H. Chen, Adsorption characteristics of both cationic and oxyanionic metal ions on hexadecyltrimethylammonium bromide-modified NaY zeolite, Chem. Eng. J., 193–194 (2012) 283–289.
[45] Y.H. Zhan, J.W. Lin, Z.L. Zhu, Removal of nitrate from aqueous solution using cetylpyridinium bromide (CPB) modified zeolite as adsorbent, J. Hazard. Mater., 186 (2011) 1972–1978.
[46] S.G. Wang, W.X. Gong, X.W. Liu, B.Y. Gao, Q.Y. Yue, Removal of fulvic acids using the surfactant modified zeolite in a fixed−bed reactor, Sep. Purif. Technol., 51 (2006) 367–373.
[47] E. Dovi, A.N. Kani, A.A. Aryee, J. Ma, J.J. Li, Z.H. Li, L.B. Qu, R.P. Han, Decontamination of bisphenol A and Congo red dye from solution by using CTAB functionalized walnut shell, Environ. Sci. Pollut. Res., 28 (2021) 28732–28749.
[48] X.F. Ren, R.D. Zhang, W.Z. Lu, T. Zhou, R.P. Han, S.L. Zhang, Adsorption potential of 2,4-dichlorophenol onto cationic surfactant-modified Phoenix tree leaf in batch mode, Desal. Water Treat., 57 (2016) 6333–6346.